

HYDRODYNAMICS OF RELATIVISTIC BLAST WAVES IN A DENSITY-JUMP MEDIUM AND
THEIR EMISSION SIGNATURE

Z. G. DAI AND T. LU

Department of Astronomy, Nanjing University, Nanjing 210093, China
E-mail: daizigao@public1.ppt.js.cn; tlu@nju.edu.cn*Accepted for Publication in the Astrophysical Journal Letters*

ABSTRACT

We analyze in detail the hydrodynamics and afterglow emission of an ultrarelativistic blast wave when it expands in a density-jump medium. Such a medium is likely to appear in the vicinity of gamma-ray bursts (GRBs) associated with massive stars. The interaction of the blast wave with this medium is described through a reverse shock and a forward shock. We show that the reverse shock is initially relativistic if the factor of a density jump (α) is much larger than 21, and Newtonian if $1 < \alpha \ll 21$. We also calculate light curves of the afterglow emission during the interaction if the reverse shock is relativistic, and find that the optical flux density initially decays abruptly, then rises rapidly, and finally fades based on a power-law, which could be followed by an abrupt decay when the reverse shock has just crossed the originally swept-up matter. Therefore, one property of an afterglow occurring in a large-density-jump medium is an abrupt drop followed by a bump in the light curve and thus provides a probe of circumburst environments. In addition, this property could not only account for the optical afterglows of GRB 970508 and GRB 000301C but also explain the X-ray afterglow of GRB 981226.

Subject headings: gamma-rays: bursts — relativity — shock waves

1. INTRODUCTION

The density distribution of circumburst environments is one of the most important issues in the theories of gamma-ray bursts (GRBs) (for review articles see Piran 1999; van Paradijs, Kouveliotou & Wijers 2000; Mészáros 2001). On one hand, it is directly pertinent to the progenitors of GRBs. Two currently popular models for the progenitors are the mergers of compact stars (neutron stars or black holes) and the explosions of massive stars. It has been argued that GRBs produced by the former model occur in a uniform interstellar medium (ISM) with density of $\sim 1 \text{ cm}^{-3}$ and GRBs in the latter model occur in pre-burst winds (Chevalier & Li 1999) and/or giant molecular clouds (Galama & Wijers 2001; Reichart & Price 2001). Thus, an environmental signature may provide a clue about the GRB progenitors. On the other hand, the environmental properties can directly influence the decay rates of afterglows. For example, afterglows arising from the interaction with pre-burst winds should decay more rapidly than afterglows do in a low-density medium (e.g., ISM) (Dai & Lu 1998a; Mészáros, Rees & Wijers 1998; Panaiteescu, Mészáros & Rees 1998; Chevalier & Li 1999, 2000). Furthermore, ultrarelativistic fireballs (or jets) in a uniform dense medium (e.g., galactic-like giant molecular clouds) must evolve to the non-relativistic regime within a few days after the bursts, leading to a rapid decay of the afterglows (Dai & Lu 1999, 2000; Wang, Dai & Lu 2000). It is thus natural that an afterglow signature can probe the ambient matter as well as the progenitors.

In the previous afterglow shock models, the environments of GRBs are usually assumed to be continuous media (e.g., ISM and wind). Actually, there are possibly jumps (or bumps) in the density profile of the ambient media of GRBs associated with massive stars. Such jumps may be produced by several astrophysical processes, e.g., the deceleration of winds in their external medium

(Ramirez-Ruiz et al. 2001; R. Wijers 2001, private communication) or the interaction of fast and slow winds (Luo & McCray 1991; Vikram & Balick 1998) or pre-burst supernova ejecta (Vietri & Stella 1998). In this Letter, we perform a careful analysis for the afterglow emission when a post-burst relativistic blast wave interacts with such a density-jump medium. We first analyze the hydrodynamics of the interaction in §2 and then discuss the afterglow signature in detail in §3. Our findings are summarized and discussed in §4.

2. HYDRODYNAMICS

Let's envision that some central energy source produces an ultrarelativistic fireball. After the internal shock emission (viz., a GRB), the fireball will start to sweep up its ambient medium, leading to an ultrarelativistic blast wave. The initial hydrodynamics of this interaction has been analyzed in detail by Sari & Piran (1995), and studied numerically by Kobayashi, Piran & Sari (1999) and Kobayashi & Sari (2000). Now we consider this ultrarelativistic blast wave which first expands in an ISM or a stellar wind and then hits an outer high-density region. We assume that the medium of interest has a simple density profile: $n = AR^{-s}$ for $R \leq R_0$ and $n = n_1 = \text{constant}$ for $R > R_0$. Here $A = n_0 \times 1 \text{ cm}^{-3}$ if the inner medium is an ISM ($s = 0$), and $A = 3 \times 10^{35} A_* \text{ cm}^{-1}$ if the inner medium is a wind ($s = 2$). Such a density profile seems to be able to reconcile the contradiction that the multiwavelength afterglow fits in the jet model by Panaiteescu & Kumar (2001) indicate an ambient medium density significantly lower than that expected in star-forming regions. Ramirez-Ruiz et al. (2001) showed that the interaction of winds from massive stars with the ambient medium can indeed lead to a large density jump at a few 10^{17} cm .

Before the blast wave hits the high-density medium, its Lorentz factor decays based on the Blandford-McKee's

(1976) solution as $\gamma = 8.2E_{53}^{1/8}n_0^{-1/8}t^{-3/8}$ in the inner-ISM case and $\gamma = 8.8E_{53}^{1/4}A_*^{-1/4}t^{-1/4}$ in the inner-wind case, where E_{53} is the energy of the blast wave in units of 10^{53} ergs and t is the observer's time in units of 1 day (neglecting the redshift effect). Subsequently, the interaction of the blast wave with the high-density medium is described through two shocks: a reverse shock that propagates into the hot shell (viz., the $R \leq R_0$ medium swept up by the blast wave), and a forward shock that propagates into the high-density medium. Therefore, there are four regions separated by the two shocks in this system: (1) unshocked high-density medium, (2) forward-shocked high-density medium, (3) reverse-shocked hot shell, and (4) unshocked hot shell. We denote n_i , e_i and p_i as the baryon number density, energy density and pressure of region “ i ” in its own rest frame respectively; γ_i and β_i are the Lorentz factor and dimensionless velocity of region “ i ” measured in the local medium’s rest frame respectively; and γ_{ij} and β_{ij} are the relative Lorentz factor and dimensionless velocity of region “ i ” measured in the rest frame of region “ j ” respectively. If $\gamma_i \gg 1$ and $\gamma_j \gg 1$, then $\gamma_{ij} \simeq (\gamma_i/\gamma_j + \gamma_j/\gamma_i)/2$. We further assume the equations of state for regions 2, 3 and 4 to be relativistic and region 1 to be cold. Thus, the equations describing the jump conditions for the forward and reverse shocks become (Blandford & McKee 1976; Sari & Piran 1995; Kumar & Piran 2000; Zhang & Mészáros 2001a)

$$\frac{e_2}{n_2 m_p c^2} = \gamma_2 - 1, \quad \frac{n_2}{n_1} = 4\gamma_2 + 3, \quad (1)$$

$$\gamma_{34}^2 = \frac{(1 + 3e_3/e_4)(3 + e_3/e_4)}{16e_3/e_4}, \quad (2)$$

$$\left(\frac{n_3}{n_4}\right)^2 = \frac{(e_3/e_4)(1 + 3e_3/e_4)}{3 + e_3/e_4}, \quad (3)$$

where m_p is the proton mass.

Regions 2 and 3 should keep the pressure equilibrium and velocity equality along the contact discontinuity, which yield $\gamma_2 = \gamma_3$ and $e_2 = e_3$. Under these conditions, the solution of equations (1)-(3) depends only on two parameters: γ_4 and $f \equiv e_4/(n_1 m_p c^2)$. The solution has two limits which correspond to the cases that the reverse shock is relativistic or Newtonian. If $e_3 \gg e_4$, then the reverse shock is initially relativistic:

$$\gamma_2 = \gamma_3 = \frac{\gamma_4^{1/2} f^{1/4}}{3^{1/4}}, \quad \gamma_{34} = \frac{3^{1/4} \gamma_4^{1/2}}{2 f^{1/4}} \gg 1, \quad (4)$$

which requires $\alpha \equiv n_1/n_0 \gg 64/3 \simeq 21$, where n_0 is the baryon number density of the inner medium at $R = R_0$ and the energy density of region 4 at this radius is assumed to equal $4\gamma_4^2 n_0 m_p c^2$. From equation (4), $\gamma_3 \ll \gamma_4$, showing that most of the initial kinetic energy of region 4 is converted into thermal energy by the shocks. On the other hand, for $1 < \alpha \ll 21$, the reverse shock is Newtonian:

$$\gamma_{34} - 1 \simeq \frac{1}{2} \left(\frac{2\gamma_4/\sqrt{f} - 1}{2\gamma_4/\sqrt{f} + 2/\sqrt{3}} \right)^2 \equiv \frac{1}{2}\xi^2, \quad (5)$$

$$\gamma_2 = \gamma_3 \simeq \gamma_4(1 - |\xi|). \quad (6)$$

In this case, the reverse shock converts only a small fraction ($|\xi| \ll 1$) of the kinetic energy into thermal energy because $2\gamma_4 \sim \sqrt{f}$. Thus, the forward shock expands almost at the velocity of the previous blast wave.

In the next section, we will discuss light curves of the afterglow emission if the reverse shock is initially relativistic. For this purpose, we need to know how the thermodynamic quantities and Lorentz factor of each region evolve with radius R at two different stages:

When the reverse shock crosses region 4, this region always expands adiabatically at a constant Lorentz factor of γ_4 , and thus we have $n_4 \propto R^{-3}$ and $e_4 \propto n_4^{4/3} \propto R^{-4}$. As a result, we obtain $f \propto R^{-4}$. For regions 2 and 3, we have $\gamma_2 = \gamma_3 \propto f^{1/4} \propto R^{-1}$, $e_2 = e_3 \propto \gamma_2^2 \propto R^{-2}$, $n_2 \propto \gamma_2 \propto R^{-1}$, and $n_3 \propto n_4 (e_3/e_4)^{1/2} \propto R^{-2}$. At this stage, $\gamma_{34} \propto R$, which is different from the initial hydrodynamics of a relativistic blast wave, $\gamma_{34} \propto R^{3/4}$, derived from Sari & Piran (1995) in the thin shell case. This is due to a hot region 4 as compared to Sari & Piran (1995).

After the reverse shock crosses region 4, the profile of the shocked high-density medium begins to approach the Blandford-McKee solution as long as the shocked matter has a relativistic equation of state, as shown numerically at the initially hydrodynamic stage of an afterglow by Kobayashi et al. (1999) and Kobayashi & Sari (2000). Using this solution, the Lorentz factor and the energy density of a given fluid element for region 3 decay as $\gamma_3 \propto R^{-7/2}$ and $e_3 \propto R^{-26/3}$ (Sari & Piran 1999a, 1999b). In addition, the Lorentz factor and the energy density of region 2 evolve as $\gamma_2 \propto R^{-3/2}$ and $e_2 \propto R^{-3}$.

3. LIGHT CURVES OF THE EMISSION

We now consider synchrotron radiation from all the regions at two different stages. The electron energy distribution just behind the shock is usually a power-law: $dn_e/d\gamma_e \propto \gamma_e^{-p}$ for $\gamma_e \geq \gamma_m$. Here we discuss only the case of $p > 2$. Dai & Cheng (2001) have discussed light curves of the emission from a relativistic shock in an ISM or a wind for $1 < p < 2$. Assuming that ϵ_e and ϵ_B are constant fractions of the internal energy density going into the electrons and the magnetic field respectively, we have the electron minimum Lorentz factor, $\gamma_{m,i} = [(p-2)/(p-1)]\epsilon_e e_i / (n_i m_e c^2)$, and the magnetic field, $B_i = (8\pi\epsilon_B e_i)^{1/2}$, for region “ i ”, where m_e is the electron mass.

According to Sari, Piran & Narayan (1998), the spectrum consists of four power-law parts with three break frequencies: the self-absorption frequency, the typical synchrotron frequency $\nu_{m,i} = \gamma_i \gamma_{m,i}^2 e B_i / (2\pi m_e c)$, and the cooling frequency $\nu_{c,i} = 18\pi e m_e c / (\sigma_T^2 B_i^3 \gamma_i t^2)$, where σ_T is the Thomson scattering cross section. In this Letter we neglect the self-absorption because it does not affect the optical radiation which we are interested in. In order to calculate the flux density at a fixed frequency, one still needs to derive the peak flux density. The observed peak flux density is given by $F_{\nu_m,i} = N_{e,i} \gamma_i P_{\nu_m,i} / (4\pi D_L^2)$, where $N_{e,i}$ is the electron number of region “ i ” at radius R , $P_{\nu_m,i} = m_e c^2 \sigma_T B_i / (3e)$ is the radiated power per electron per unit frequency in the frame comoving with the shocked matter, and D_L is the source’s luminosity distance to the observer. So we in fact need to calculate $N_{e,i}$. First, it is easy to obtain the total electron number of region 2

by $N_{e,2} = (4\pi/3)n_1(R^3 - R_0^3)$. Second, the time interval for the reverse shock to spend in crossing a length interval dx'_4 in the rest frame of region 4 is $dt'_4 = dx'_4/(\beta_{34}c)$, which is related to a time interval (dt'_3) in the rest frame of region 3 by $dt'_4 = \gamma_{34}dt'_3$, and furthermore dt'_3 is related to a time interval (dt_m) in the local medium's rest frame by $dt'_3 = dt_m/\gamma_3 = dR/(\gamma_3\beta_3c)$, so we calculate the electron number of region 3: $N_{e,3} = \int_0^{x'_4} 4\pi R^2 n_4 dx'_4 = \int_{R_0}^R 4\pi R^2 n_4 [\gamma_{34}\beta_{34}/(\gamma_3\beta_3)] dR \propto (R^2 - R_0^2)$, where $\beta_{34} \approx \beta_3 \approx 1$, and thus the electron number of region 4 is $N_{e,4} = 4\pi A R_0^{3-s}/(3-s) - N_{e,3}$, when the reverse shock crosses region 4. Letting $N_{e,3}$ equal the initial electron number of region 4 (viz., when $N_{e,4} = 0$), we can calculate the radius at which the reverse shock has just crossed this region: $R_\Delta = R_0(1 + 5.83 \times 10^{-3} n_0^{1/2} n_{1,3}^{-1/2})$ for $s = 0$ and $R_\Delta = R_0(1 + 1.25 \times 10^{-2} E_{53}^{-1/2} A_* n_{1,3}^{-1/2} t_0^{-1/2})$ for $s = 2$, where $n_{1,3} = n_1/10^3 \text{ cm}^{-3}$ and t_0 is the observer's time (in 1 day) at $R = R_0$.

Although the spectrum does not depend on the hydrodynamics of the shocked matter, the light curve at a fixed frequency is determined by the temporal evolution of $\nu_{m,i}$, $\nu_{c,i}$ and $F_{\nu_{m,i}}$. These quantities depend on how γ_i , n_i , e_i and $N_{e,i}$ scale as a function of R as well as t either for $R_0 \leq R \leq R_\Delta$ or for $R > R_\Delta$. However, we note that for the typical values of the involved parameters (see below), $R_\Delta/R_0 - 1 \ll 1$, showing that γ_i , n_i and e_i are almost unchanged and thus we consider only the temporal evolution of $\nu_{c,i}$ ($\propto t^{-2}$) and $N_{e,i}$ for $R_0 \leq R \leq R_\Delta$.

One crucial effect in calculating the light curve is that the photons which are radiated from different regions at the same time measured in the local medium's rest frame will be detected at different observer times (Zhang & Mészáros 2001a). The understanding of this effect is that for $R_0 \leq R \leq R_\Delta$ the Lorentz factor of region 4 is much larger than that of regions 2 and 3 so that for a same time interval in the local medium's rest frame, dR/c , the emission from region 4 reaches the observer in a time interval of $\sim dR/(2c\gamma_4^2)$, while the emission from regions 3 and 2 reaches the observer in a time interval of $\sim dR/(2c\gamma_3^2)$. After considering this effect and the scaling law of γ_i with R , we obtain the observer time of the radiation from region 4 at $R = R_\Delta$: $t_{\Delta,4} = t_0(1 + 1.16 \times 10^{-2} n_0^{1/2} n_{1,3}^{-1/2})$ for $s = 0$ and $t_{\Delta,4} = t_0(1 + 2.50 \times 10^{-2} E_{53}^{-1/2} A_* n_{1,3}^{-1/2} t_0^{-1/2})$ for $s = 2$, and the corresponding observer time of the radiation from regions 3 and 2: $t_{\Delta,3} = 1.33t_0$ for $s = 0$ and $t_{\Delta,3} = 2.0t_0$ for $s = 2$, where we have used $R_\Delta/R_0 - 1 \ll 1$. It is thus seen that $t_{\Delta,4}/t_0 - 1 \ll t_{\Delta,3}/t_0 - 1$, implying that the observed radiation from regions 3 and 2 is indeed delayed as compared with that from region 4.

Fig. 1 presents two R-band ($\nu_R \simeq 4.4 \times 10^{14} \text{ Hz}$) light curves about the effect of an ultrarelativistic blast wave interacting with a density-jump medium on the afterglow. The outer-medium density assumed here, $n_1 \sim 10^3 \text{ cm}^{-3}$, is the one of typical galactic-like giant molecular clouds. It can be seen from this figure that at $t \geq t_0$ the flux density (F_{ν_R}) initially drops abruptly, then rises rapidly, and finally declines based on a power-law followed by an abrupt decay at $t = t_{\Delta,3}$. This result is easily understood: an initially abrupt decay of the emission is due to the spectral cutoff frequency $\nu_{\text{cut},4} < \nu_R$

(solid line) or the rapid decrease of the electron number in region 4, $N_{e,4} \propto [4t_{\Delta,4}/t_0 - (t/t_0 + 1)^2]$ (dashed line), during the adiabatic expansion for $t_0 \leq t \leq t_{\Delta,4}$. Note that $\nu_{\text{cut},4} = \nu_{c,0}(R/R_0)^{-4}$ results from evolution of the fast-cooling electrons of region 4, where $\nu_{c,0} = 2.8 \times 10^{13} \epsilon_{B,-1}^{-3/2} E_{53}^{1/2} n_0^{-1} t_0^{-1/2} \text{ Hz}$ is the cooling frequency of the originally swept-up electrons at $t = t_0$. In the period of $t_0 \leq t \leq t_{\Delta,4}$, the emission flux densities from regions 2 and 3 are low both because the two shocks have swept up only a small number of the electrons and because the radiation from these regions reaches the observer at a later time than the radiation from region 4 does. As the number of the electrons swept up by the two shocks increases, the flux density increases rapidly as $F_{\nu_R} \propto (t/t_0 - 1)(t/t_0)^{-1}$, where the first factor arises from $F_{\nu_{m,i}} \propto (t/t_0 - 1)$ and the second factor from $\nu_{c,i} \propto (t/t_0)^{-2}$ for regions 2 and 3. However, since $\nu_{c,3} < \nu_{m,3} < \nu_R$ for the parameters shown in the figure, all the electrons in region 3 are in the fast cooling regime. As a result, the R-band flux density of the radiation from this region disappears at $t \geq t_{\Delta,3}$ and thus only the radiation from region 2 could be detected. Therefore, an abrupt decay of the flux density could appear at $t = t_{\Delta,3}$. We further define the factor of emission brightening (\mathcal{R}) as the ratio of the observed density fluxes with and without a density jump at $t = t_{\Delta,3}$. In Fig. 1, $\mathcal{R} \sim 5.1$ (solid line) and $\mathcal{R} \sim 10$ (dashed line). Fig. 2 exhibits the light curves of the afterglow emission when the inner medium at $R \leq R_0$ is a stellar wind. In this figure, $\mathcal{R} \sim 5.3$ (solid line) and $\mathcal{R} \sim 11$ (dashed line). Recently Ramirez-Ruiz et al. (2001) also estimated $\mathcal{R} \sim \alpha^{(p+1)/[4(4-s)]} \simeq 4.5$ and 21 for $s = 0$ and $s = 2$ (where $p = 2.5$ and $\alpha = 10^3$) respectively. However, we find that \mathcal{R} depends on the shock parameters (e.g., ϵ_e and ϵ_B) for a fixed density jump. One reason for the difference between our and Ramirez-Ruiz et al.'s (2001) results is that for $t_0 < t < t_{\Delta,3}$ the optical emission arises partially from the reverse shock considered here. Another reason is that the electrons which produce the optical emission may be in different radiation regimes before and when the reverse shock crosses region 4.

4. DISCUSSION AND CONCLUSIONS

We have analyzed the hydrodynamics and afterglow emission of an ultrarelativistic blast wave when it interacts with a density-jump medium. This interaction is described through two shocks: a reverse shock and a forward shock. We have shown that the reverse shock is initially relativistic if $\alpha \gg 21$, and Newtonian if $1 < \alpha \ll 21$. We have also investigated in detail light curves of the afterglow emission during the interaction if the reverse shock is relativistic, and found that the R-band flux density initially decays abruptly, then rises rapidly, and finally fades based on a power-law, which could be followed by an abrupt decay when the reverse shock has just crossed the originally swept-up matter.

Our analysis is based on several simplifications: First, we have considered only one density jump, but our discussion should be in principle applied to a more realistic case in which there could be a few jumps (or bumps) in the density profile. Second, since the Y parameter for synchrotron self-Compton (SSC) is not far larger than unity in our model, the effect of SSC on the optical emission is insignificant. This effect was recently discussed by several

authors (e.g., Waxman 1997; Wei & Lu 1998; Panaiteescu & Kumar 2000; Sari & Esin 2001; Zhang & Mészáros 2001b). Third, we have assumed a spherical relativistic blast wave, but an actual blast wave may be a jet, whose edge effect and sideways expansion can lead to a steepening of the light curve (Mészáros & Rees 1999; Rhoads 1999; Sari, Piran & Halpern 1999; Dai & Cheng 2001). Fourth, we have neglected the emission off the line of sight. Such emission could significantly alleviate the initial abrupt drop of the flux density.

The humps have been observed to appear in the light curves of several optical afterglows (e.g., GRB 970508 and GRB 000301C). In our model, these humps are understood to be due to the contribution of the radiation from regions 2 and 3 when the reverse shock crosses region 4. A few other interpretations have been proposed, e.g., refreshed shocks due to Poynting-flux-dominated or kinetic-energy-dominated injection (Dai & Lu 1998b; Panaiteescu, Mészáros & Rees 1998; Zhang & Mészáros 2001a, 2001c; Chang et al. 2001), and microlensing events (Garnavich, Loeb & Stanek 2000). However, there is not any abrupt drop in the afterglow light curves of the latter models. This property could be used to distinguish between the present model and the other interpretations. We will carry out detailed fits to the optical afterglows of GRB 970508

and GRB 000301C based on the present model. In addition, this model can account well for the rise-decline feature of the X-ray afterglow light curve of GRB 981226 (Frontera et al. 2000).

Finally, we have noted that when the reverse shock crosses region 4, neutrinos with energies of TeV-PeV are possibly produced by π^+ created in interactions between accelerated protons and synchrotron photons from accelerated electrons in regions 2 and 3. Furthermore, such neutrino emission is delayed about $t_{\Delta,3}$ after the GRB. This result is different from the prompt neutrino emission discussed by many authors, e.g., Waxman & Bahcall (1997, 2000), Bahcall & Mészáros (2000), Mészáros & Rees (2000), Dai & Lu (2001), and Mészáros & Waxman (2001). One expects that these delayed neutrinos, if detected, could provide further diagnostics about circum-burst density-jump environments.

We thank Ralph Wijers for valuable discussions, and Y. F. Huang, X. Y. Wang, B. Zhang and the referee for useful comments. We particularly thank B. Zhang for careful reading the manuscript. This work was supported by the National Natural Science Foundation of China (grants 19825109 and 19773007) and the National 973 Project (NKBRSF G19990754).

REFERENCES

Bahcall, J. N., & Mészáros, P. 2000, Phys. Rev. Lett., 85, 1362
 Blandford, R. D., & McKee, C. F. 1976, Phys. Fluids, 19, 1130
 Chang, H. Y., Lee, C. H., & Yi, I. 2001, A&A Lett., in press (astro-ph/0110640)
 Chevalier, R. A., & Li, Z. Y. 1999, ApJ, 520, L29
 Chevalier, R. A., & Li, Z. Y. 2000, ApJ, 536, 195
 Dai, Z. G., & Cheng, K. S. 2001, ApJ, 558, L109
 Dai, Z. G., & Lu, T. 1998a, MNRAS, 298, 87
 ———. 1998b, Phys. Rev. Lett., 81, 4301
 ———. 1999, ApJ, 519, L155
 ———. 2000, ApJ, 537, 803
 ———. 2001, ApJ, 551, 249
 Frontera, F. et al. 2000, ApJ, 540, 697
 Galama, T. J., & Wijers, R. A. M. J. 2001, ApJ, 549, L209
 Garnavich, P., Loeb, A., & Stanek, K. 2000, ApJ, 544, L11
 Kobayashi, S., Piran, T., & Sari, R. 1999, ApJ, 513, 669
 Kobayashi, S., & Sari, R. 2000, ApJ, 542, 819
 Kumar, P., & Piran, T. 2000, ApJ, 532, 286
 Luo, D., & McCray, R. 1991, ApJ, 379, 659
 Mészáros, P. 2001, to appear in ARA&A (2002) (astro-ph/0111170)
 Mészáros, P., & Rees, M. J. 1999, MNRAS, 306, L39
 ———. 2000, ApJ, 541, L5
 Mészáros, P., & Waxman, E. 2001, Phys. Rev. Lett., 87, 1102
 Mészáros, P., Rees, M. J., & Wijers, R. A. M. J. 1998, ApJ, 499, 301
 Panaiteescu, A., & Kumar, P. 2000, ApJ, 543, 66
 ———. 2001, ApJ, in press (astro-ph/0109124)
 Panaiteescu, A., Mészáros, P., & Rees, M. J. 1998, ApJ, 503, 314
 Piran, T. 1999, Phys. Rep., 314, 575
 Ramirez-Ruiz, E., Dray, L. M., Madau, P., & Tout, C. A. 2001, MNRAS, in press (astro-ph/0012396)
 Reichart, D. E., & Price, P. A. 2001, ApJ, in press (astro-ph/0107547)
 Rhoads, J. 1999, ApJ, 525, 737
 Sari, R., & Esin, A. A. 2001, ApJ, 548, 787
 Sari, R., & Piran, T. 1995, ApJ, 455, L143
 ———. 1999a, ApJ, 517, L109
 ———. 1999b, ApJ, 520, 641
 Sari, R., Piran, T., & Halpern, J. P. 1999, ApJ, 519, L17
 Sari, R., Piran, T., & Narayan, R. 1998, ApJ, 497, L17
 van Paradijs, J., Kouveliotou, C., & Wijers, R. A. M. J. 2000, ARA&A, 38, 379
 Vietri, M., & Stella, L. 1998, ApJ, 507, L45
 Vikram, D., & Balick, B. 1998, ApJ, 497, 267
 Wang, X. Y., Dai, Z. G., & Lu, T. 2000, MNRAS, 317, 170
 Waxman, E. 1997, ApJ, 485, L5
 Waxman, E., & Bahcall, J. N. 1997, Phys. Rev. Lett., 78, 2292
 ———. 2000, ApJ, 541, 707
 Wei, D. M., & Lu, T. 1998, ApJ, 505, 252
 Zhang, B., & Mészáros, P. 2001a, ApJ, 566, in press (astro-ph/0108402)
 ———. 2001b, ApJ, 559, 110
 ———. 2001c, ApJ, 552, L35

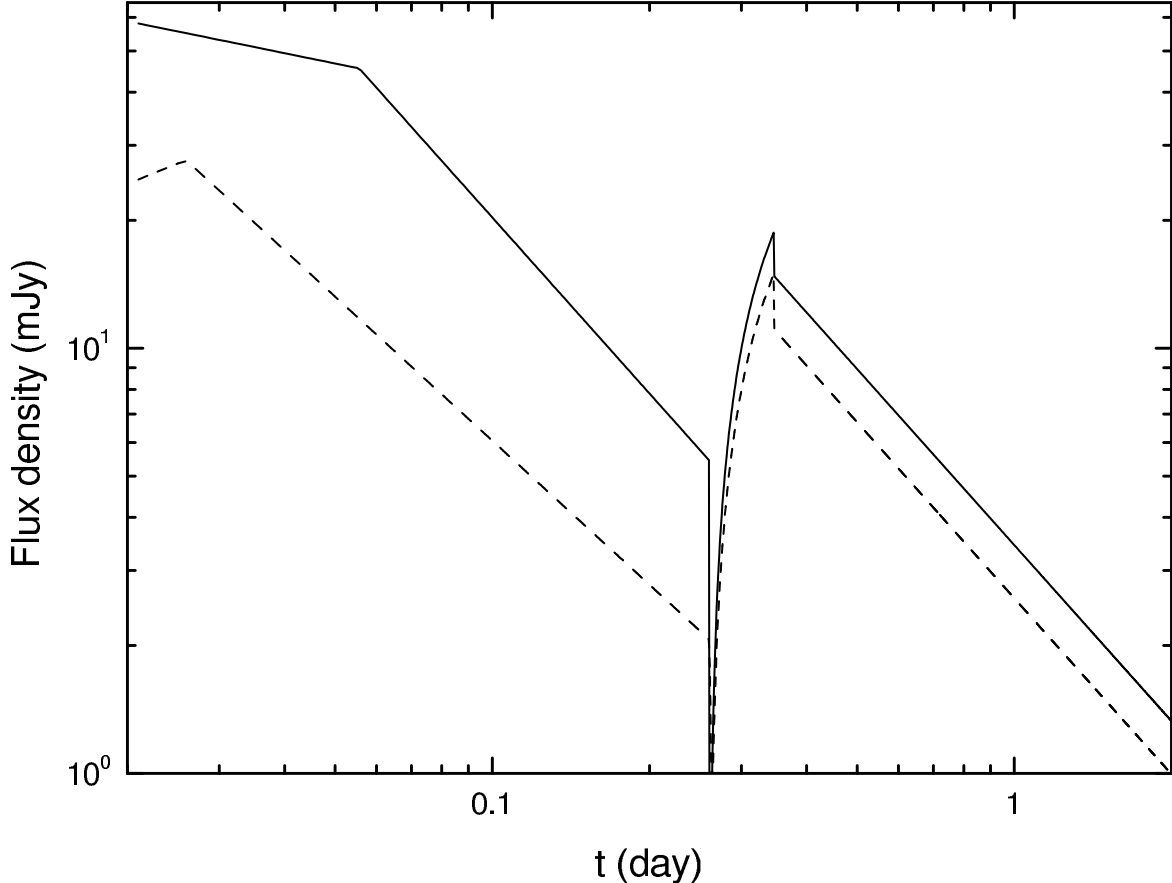


FIG. 1.— R-band light curves of the afterglow emission when an ultrarelativistic blast wave interacts with a density-jump medium. The blast wave expands within an ISM ($s = 0$) until it reaches a high-density medium at $R_0 = 5 \times 10^{17}$ cm (or $t_0 = 0.26$ days). The model parameters are taken: $E_{53} = 1$, $n_0 = 1$, $n_{1,3} = 1$, $\epsilon_e = 0.1$, $p = 2.5$ and $D_L = 2 \times 10^{28}$ cm. The solid and dashed lines correspond to $\epsilon_B = 0.1$ and 0.01 respectively.

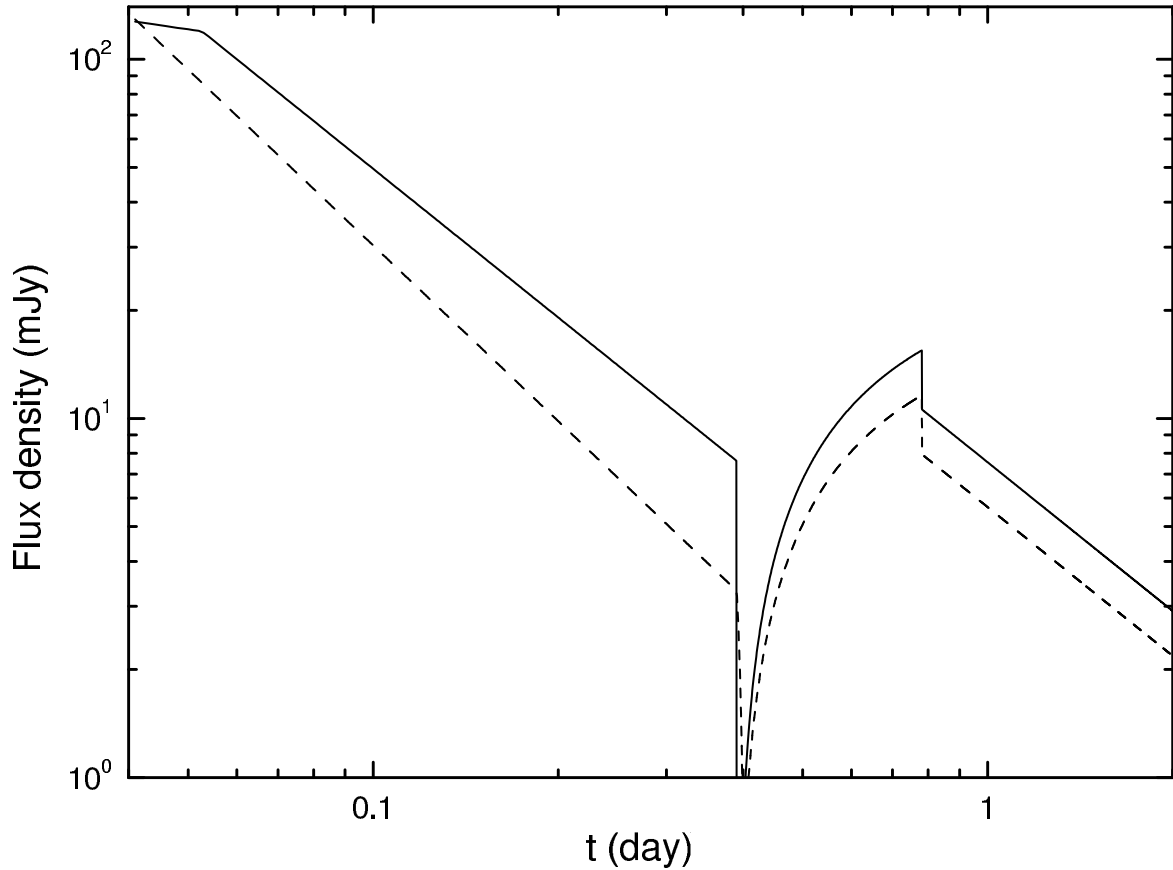


FIG. 2.— Same as Fig. 1 but the inner medium at $R \leq R_0 = 5 \times 10^{17}$ cm is a stellar wind ($s = 2$) with $A_* = 1$ and $t_0 = 0.39$ days.